Macromolecular Research, Vol. 25, No. 4, pp 365-373 (2017)
DOI 10.1007/s13233-017-5041-9

www.springer.com/13233
pISSN 1598-5032 eISSN 2092-7673

Structural, Thermal, and Tribological Properties of Poly(vinylidene fluoride)/ Nano-TiO_2 Composites Prepared by Dry-Mixing and Hot-Press Technique

Jung Pyo Jung[1], Ji-Su Kim[2], Tong-Seok Han[2], and Jong Hak Kim*[,1]

[1]*Department of Chemical and Biomolecular Engineering, Yonsei University, 50 Yonsei-ro, Seodaemun-gu, Seoul 03722, Korea*
[2]*Department of Civil and Environmental Engineering, Yonsei University, 50 Yonsei-ro, Seodaemun-gu, Seoul 03722, Korea*

Received November 1, 2016; Revised December 11, 2016; Accepted December 18, 2016

Abstract: This paper describes the morphological, thermal, and tribological characteristics of poly(vinylidene fluoride) (PVDF)-based composites dispersed with nanosized TiO_2 (nano-TiO_2) particles. PVDF/nano-TiO_2 composites with different nano-TiO_2 loading (~40 wt%) were prepared *via* a dry-mixing and uniaxial hot-press molding technique. The incorporation of nano-TiO_2 led to changes in the crystal structure of the PVDF, as characterized by Fourier transform infrared spectroscopy, X-ray diffraction, thermogravimetric analysis, and differential scanning calorimetry. The uniform distribution and good interactions of the composites were confirmed by scanning electron microscopy and energy-dispersive spectrometry. The frictional performances increased with the amount of nano-TiO_2 owing to the preferential formation of a nonpolar α-phase crystal and the reduced viscoelastic characteristics of the PVDF. The PVDF/nano-TiO_2 composite with 30% loading exhibited the best frictional performance (a static-friction coefficient of 0.23 and a kinetic-friction coefficient of 0.17), which is comparable to that of the composite prepared *via* a costly, environmentally unfriendly wet-mixing technique. Furthermore, the taber abrasion resistances were comparable to that of commercialized ultra-high-molecular-weight polyethylene (UHMWPE), indicating the effectiveness of PVDF/nano-TiO_2 hybridization.

Keywords: composite, poly(vinylidene fluoride), TiO_2, friction coefficient, taber abrasion.

Introduction

Polymer composites consist of inorganic nanofillers dispersed in a polymer matrix. In particular, composites containing metal oxides have been extensively researched owing to their versatile applications in several areas, including electrochemistry, photovoltaics, catalysis, and membrane separation.[1-4] A variety of morphologies comprising metal oxides have been used, such as nanoparticles, nanotubes, nanorods, nanowires, nanoflakes, and nanosheets.[5,6] For superior properties, at least one dimension must preferably lie in the size range below 50 nm. This is because the change in dimensions and the transition from microsize to nanosize leads to a significant change in the physicochemical properties. As the specific surface area of the nanofiller increases, the interaction between the filler and the polymer matrix is strengthened, thereby enhancing the mechanical and thermal properties of the composites.

Base isolation is known to be one of the most effective approaches for the seismic-hazard mitigation of infrastructural systems. The base isolation system is a seismic design method that reduces the earthquake load in order to elongate the fundamental period of a structure. There were several studies on the effect of the base isolation according to the geometry of concave slide and the property of frictional materials.[7,8] Many previous studies involved parametric analyses with different friction coefficients using analytical methods. Additionally, researchers have focused on the control of the friction coefficient, reporting that a low friction coefficient can lead to high seismic performance. In the present study, a new composite material for an isolation device is investigated. The purpose of the study is to develop a class of frictional materials with an on-demand frictional coefficient for satisfying the required seismic performance of the base isolation system.

Recently, considerable attempts have been made to develop polymer composites containing an inorganic nanofiller to improve their thermal and tribological properties.[9-12] Many studies have focused on composites based on poly(tetrafluoroethylene) (PTFE) owing to its good mechanical, thermal, and chemical properties.[13-18] As a matrix of the frictional material, PTFE coating is effective in yielding a low friction coefficient and a relatively high wear resistance.[17] It has been reported that the friction coefficient and wear rate are reduced while the corrosion resistance is improved by the incorporation of inorganic fillers such as ZnO,[13] SiO_2,[14] Al_2O_3,[15] graphene

*Corresponding Author. E-mail: jonghak@yonsei.ac.kr

oxide,[16] Ni-W,[17] and MoS_2.[18] In addition, many studies have examined the performance of composites based on poly(ether ether ketone) (PEEK).[19-22] For example, Kalin *et al*. investigated the effect of the type of nanoparticles on the mechanical properties of PEEK composites.[19] The tribological performances of PEEK hybrid composites reinforced with short carbon fibers and surface modified nano-SiO_2 particles were systematically investigated.[20,21]

Poly(vinylidene fluoride) (PVDF) is a partially fluorinated polymer that is considered a suitable alternative to the fully fluorinated PTFE because of its much lower cost, better processability, and good solubility in solvents.[23-25] However, the preparation of PVDF-based composites for applications involving wear, friction, and tribological performances has rarely been reported.[26,27] Thus, in the present study, a series of polymer composites were prepared using PVDF and nano-sized TiO_2 (nano-TiO_2) particles as the matrix and filler, respectively, *via* a dry-mixing and uniaxial hot-press molding technique. By changing the amounts of nano-TiO_2 fillers, several physicochemical analyses, including Fourier transform infrared spectroscopy (FTIR), scanning electron microscopy (SEM), energy dispersive spectrometry (EDS), X-ray diffraction (XRD), thermogravimetric analysis (TGA), and differential scanning calorimetry (DSC) were conducted to investigate the properties of developed materials. Furthermore, mechanical analyses including the abrasive wear performance and frictional performance were conducted for evaluating the tribological performance.

Experimental

Materials. PVDF (weight-average molecular weight (M_w) ~534,000 g mol^{-1}) was purchased from Sigma-Aldrich. TiO_2 (Aeroxide®) - a fine-particulate, pure titanium dioxide - was obtained from Evonik Co., Ltd.

Fabrication of PVDF/Nano-TiO_2 Composites. Neat PVDF and PVDF/nano-TiO_2 composite films were prepared *via* dry-mixing and uniaxial hot-pressing. For the preparation of the PVDF film, PVDF powder was placed onto a square-shaped mold, and then 20 MPa of pressure was applied at 190 °C. After 30 min of pressing, the mold was cooled to room temperature under continuous pressing. To prepare the PVDF/nano-TiO_2 composite films, PVDF and nano-TiO_2 powders were mixed in various weight ratios by vigorous stirring for 1 day. Then, an ultra-sonication process was conducted for the mixed powders to minimize the agglomeration of each powder. Thus, the same fabrication method used for the preparation of the PVDF film was applied. The PVDF/nano-TiO_2 composite films were prepared by uniaxial hot-pressing at 190 °C at 20 MPa for 30 min and cooled to room temperature under continuous pressing.

Characterization. FTIR data were obtained from an Excalibur series FTIR instrument (DIGLAB Co., Hannover, Germany) in the frequency range of 4000-500 cm^{-1}. XRD measurements were conducted using a Rigaku RINT2000 wide-angle goniometer with a Cu cathode operated at 40 kV and 300 mA. DSC curves were measured using a differential scanning calorimeter (DSC8000 Perkin Elmer, USA) to analyze the thermal behavior of the systems at a heating rate of 10 °C/min in a nitrogen atmosphere. The systems were heated from 25 to 330 °C, and scanned thermogram information was used to determine the crystalline melting temperature (T_m) and thermal-degradation temperature of the systems. TGA was performed with a simultaneous DTA/TGA analyzer (TA Instruments, USA) at a heating rate of 10 °C/min rate in a nitrogen atmosphere. The cross-sectional morphology and EDS mapping of the composites were characterized using a field-emission scanning electron microscope (SUPAR 55VP, Carl Zeiss, Germany).

Mechanical Test for Tribological Properties. Three different types of property analyses were conducted: a density measurement, coefficient-of-friction test, and wear-resistance test. Each test followed the standard test method (ASTM, KS), and the same testing conditions were maintained during several tests with different specimens. The following are brief descriptions of these test methods.

The density was measured to verify the prepared specimens with different amounts of nano-TiO_2. The pure densities of PVDF and nano-TiO_2 differed so that the density of the composite could be changed according to the amount of filler. The theoretical density was calculated, and two theoretical and experimental results were compared. The density of the specimen was obtained using an electronic densimeter (MD-300S, Alfa Mirage Co., Osaka, Japan) at 23 °C. This test followed ASTM D 792, which is a standard for the determination of the specific gravity and relative density. The ASTM D 792 summarizes the test method as follows. After determining the mass of a specimen in air, it was immersed in a liquid, and its apparent mass upon immersion was determined. Then, the specific gravity or relative density was obtained. Three specimens with the same amounts of nano-TiO_2 were used, to ensure the reliability of the density measurement.

The friction coefficient was determined using ASTM D 1894, which is a standard test method for the static and kinematic coefficients of friction of plastic film and sheeting. This test was conducted by using a universal testing machine with a velocity of 150 mm/min and a load cell of 5 N. The temperature and relative humidity for the test were 25 °C and 45%, respectively. The friction coefficient was determined according to SUS304. The vertical load was 2.25 N, the specimen was square-shaped with edges 6.3 cm long. The friction coefficient depended on the conditions of the specimen surface and the vertical load.

The wear rate was determined according to a taber wear test, on the basis of KS M ISO 9352. This test was conducted by using wheels to create a circular wear path. A taber abrasion tester (Yasuda LTD., Hyogo, Japan) was used, and a CS-17 wheel was applied with operated loads of 500 g. The test

involved a 3,000-cycle (diameter=4.45 cm) displacement history with 60 rpm. The temperature and relative humidity were 25 °C and 45%, respectively.

Results and Discussion

Preparation and Structure of Composites. A series of composite films with a thickness of 3 mm and various nano-TiO_2 loading values were prepared *via* the dry-mixing and uniaxial hot-press technique, as shown in Figure 1. The wet-mixing process can be more effective for producing composites with intimate contact[28,29] but is costly owing to the necessity of a large amount of liquid solvent. In our study, to overcome the disadvantage of dry-mixing, an ultra-sonication process was employed, which induced the homogeneous distribution of the filler and the intimate contact of the composites. It was also important to use fine powders for the filler and the matrix. The high molecular weight of PVDF (534,000 g mol^{-1}), which is far higher than its entanglement molecular weight, was also responsible for the good mechanical properties of the composite films. The neat PVDF film was transparent, bendable, and mechanically strong. The films gradually became opaque with the addition of nano-TiO_2 (Figure 1(a)), which is because the refractive index of PVDF (1.42) is significantly different from that of TiO_2 (2.88 at 632 nm), and thus a large amount of light was scattered at the PVDF/nano-TiO_2 interface. It has been reported that the incorporation of TiO_2 enhances the refractive index of polymer composites.[30] The excess amount of nano-TiO_2 (*e.g.*, 50 wt%) led to the partial aggregation of nano-TiO_2 and the fragility of the composite films (Figure 1(b)).

Figure 2 shows the FTIR spectra of PVDF powder, PVDF film, and PVDF/nano-TiO_2 composite films. The powder sample was measured and compared in order to investigate the effect of hot-pressing on the polymer structure. PVDF can exist in three different crystalline forms - α (TGTG'), β (TTTT), and γ (TTTGTTTG') phases - depending on the chain conformations with trans (T) or gauche (G) linkages, as shown in Figure 3.[31] The α phase is nonpolar, as the anti-parallel packing of the dipoles contributes to a zero-sum dipole moment.

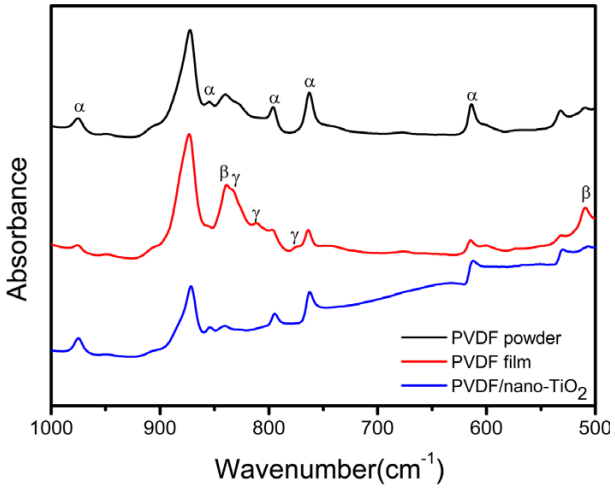

Figure 2. FTIR spectra of PVDF powder, PVDF film, and PVDF/nano-TiO_2 composite film with TiO_2 loading of 30 wt%.

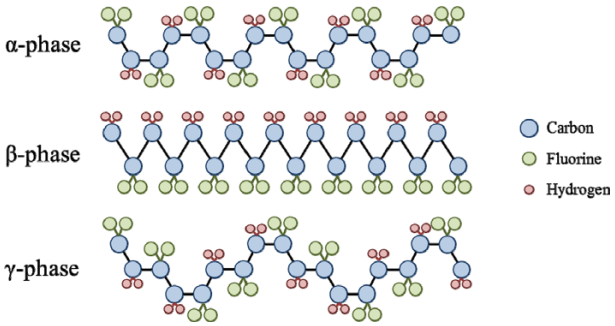

Figure 3. Schematic representation for α, β, and γ phases of PVDF.

On the other hand, the β and γ phases have high dipole moments because of their structural arrangement. For all three samples, several absorption bands were observed at 975, 855, 796, and 763 cm^{-1} owing to the characteristic bands of the α-phase PVDF.[32-34] The characteristic absorption bands of β-phase PVDF at 840 and 510 cm^{-1} were observed for all the samples. However, the intensities of the α-phase absorption bands were relatively strong for the neat PVDF powder,

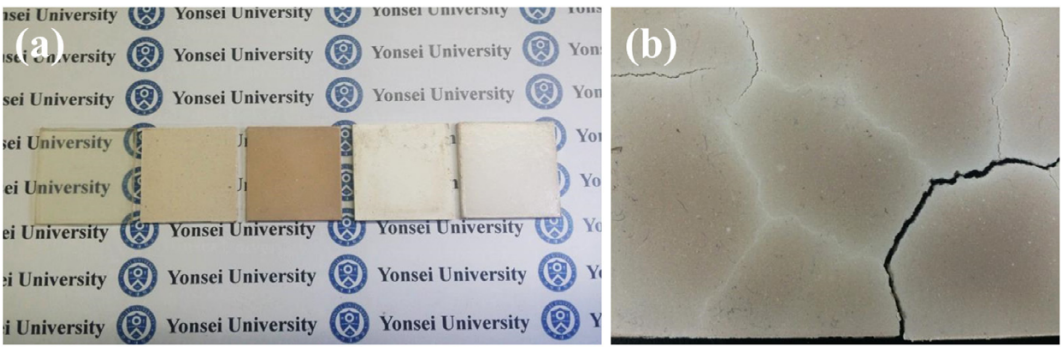

Figure 1. Photographs of (a) neat PVDF film and PVDF/nano-TiO_2 composite films (from left, in the order of nano-TiO_2 loading of 0, 10, 20, 30, and 40 wt%) and (b) PVDF/nano-TiO_2 composite film with nano-TiO_2 loading of 50 wt%.

whereas the β-phase and γ-phase absorption bands became intense for the PVDF film prepared by uniaxial hot-pressing, indicating the conformational rearrangement of chains during the process.[32-34] It has been reported that the β-phase crystal of PVDF can be transformed from the α-phase crystal by mechanical deformation and thermal annealing, which provides excellent pyro- and piezoelectric properties of PVDF.[33,34] Upon incorporation of nano-TiO_2, both the β-phase and γ-phase absorption bands became weak, indicating that the α-phase crystal was dominant for the PVDF/nano-TiO_2 composites. The PVDF film was prepared by hot-pressing, which involved mechanical and thermal deformation; thus, strong dipole-induced attraction occurred, forming a polar β-phase crystal. This led to reduced voids among the macromolecular chains. However, the nano-TiO_2 played a role as an inorganic filler to reduce the secondary bonding interactions among PVDF chains; thus, the nonpolar α-phase crystal became predominant again in the composites.

The densities of the PVDF/nano-TiO_2 composites with various amounts of TiO_2 were measured, as shown in Figure 4. Theoretical values of the density were also calculated using the following equation:

$$\rho = V_a\rho_a + (1 - V_a)\rho_{Polym} \quad (1)$$

where ρ is the density of the composites; V_a is the volume fraction of the additive; and ρ_a and ρ_{Polym} are the densities of additive and polymer matrix, respectively. The density of neat nano-TiO_2 powder is 4.26 g/cm^3, which is far larger than that of neat PVDF powder (1.74 g/cm^3); thus, the density of the PVDF/nano-TiO_2 composites gradually increased with the amount of nano-TiO_2. However, the difference between the theoretical and experimental density values became large at nano-TiO_2 contents above 20 wt%. This is because the theoretical values were calculated according to the assumption that no voids and defects existed in the composites. However, some voids and defects could be formed in a real system during the fabrication process, resulting in a reduced density.[35] The experimental density linearly increased with the nano-TiO_2 content, but the increase from 30 to 40 wt% was negligible. This indicates that the voids and defects started to form excessively at 40 wt% loading, where a difference of ~0.3 g/cm^3 between the theoretical and experimental densities was obtained. It is also interesting to note that the experimental density of 1.77 g/cm^3 observed for the PVDF film without nano-TiO_2 was slightly greater than the theoretical value of 1.74 g/cm^3. This might be because the distance and voids among the PVDF chains decreased owing to the formation of a β-phase crystal domain with a high polarity by the hot-pressing involving mechanical and thermal deformation.

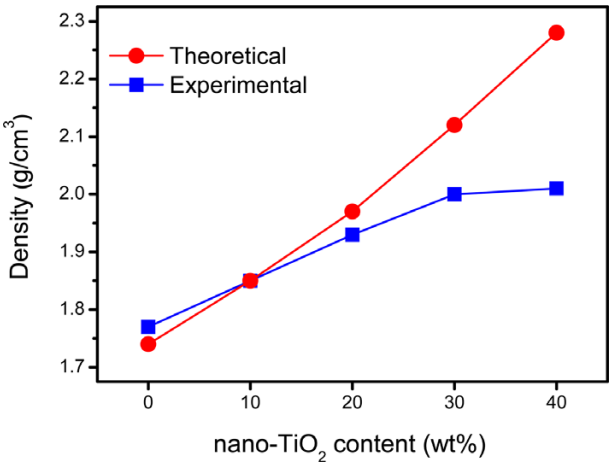

Figure 4. Density of neat PVDF film and PVDF/nano-TiO_2 composite films.

Morphological and Structural Properties. The cross-sectional morphology and the dispersion of the nano-TiO_2 filler within the PVDF matrix were characterized by SEM and EDS analysis, as shown in Figure 5. Overall, the neat PVDF film without nano-TiO_2 was smooth, and the green regions (fluorine, F) were uniformly distributed, interconnected with each other, and interlaced with the dark regions (C and H) in the microscale range. The PVDF/nano-TiO_2 composites became rougher as the amount of nano-TiO_2 filler increased. Although EDS mapping data can be affected by the height difference of the cross-sections, it is clear that the Ti element was uniformly and homogeneously dispersed throughout the PVDF matrix. The amount of Ti gradually increased with the nano-TiO_2 loading in the composites. However, the area of Ti atoms enlarged and aggregated at 40 wt% loading, which is consistent with the aforementioned density results indicating that the voids and defects started to excessively form at 40 wt% loading.

Figure 6 shows the XRD patterns of the PVDF film and PVDF/nano-TiO_2 composite films with various nano-TiO_2 loading values. The neat PVDF film exhibited strong crystalline peaks as well as a broad amorphous pattern, indicating its semi-crystalline nature. The XRD peaks observed at 2θ=17.8°, 18.4°, 20.0°, and 26.6° are assigned to the (100), (020), (110), and (021) reflections of the α-phase crystal PVDF, respectively. The peaks at 2θ=20.0° and 20.5° are attributed to the (110) and (200) reflections, respectively, of the β-phase crystal PVDF.[34,36] The peak at 20.3° represents the (101) reflection of the γ-phase crystal PVDF. All the α, β, and γ phases were observed for the PVDF film, which is consistent with the aforementioned FTIR spectroscopic results. In the case of the PVDF/nano-TiO_2 composite, several sharp peaks additionally appeared owing to the crystalline phase of nano-TiO_2. The diffraction peaks at 2θ=25.0°, 37.6°, 47.7°, 53.7°, and 54.3° are assigned to the (101), (004), (200), (105), and (211) reflections of anatase TiO_2. Diffraction peaks were also observed at 2θ=26.9°, 35.9°, 40.9°, and 43.7°, which are attributed to the (110), (101), (111), and (210) reflections of rutile TiO_2.[37,38] A comparison between the relative intensity of the XRD peaks reveals that anatase-phase TiO_2 is predominant in PVDF/nano-TiO_2 composite films. As the amount of nano-TiO_2

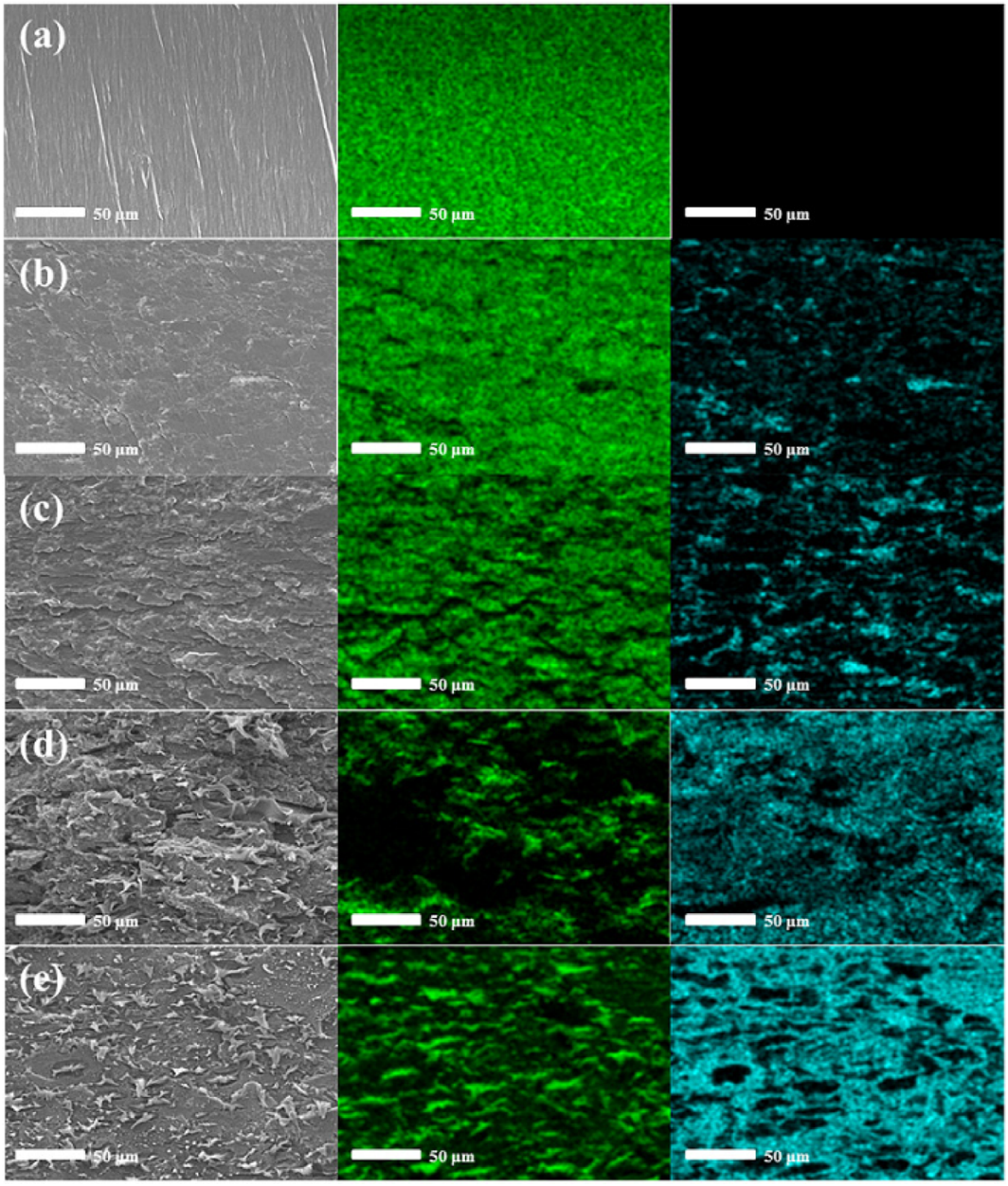

Figure 5. SEM and EDS mapping on cross-sectional images of neat PVDF film and PVDF/nano-TiO_2 composite films: (a) neat PVDF, (b) nano-TiO_2 10 wt%, (c) 20 wt%, (d) 30 wt%, and (e) 40 wt%, green: F element, blue: T element.

increased, the peak intensity of the PVDF matrix decreased, while the peak intensity of the TiO_2 phases increased. Interestingly, the relative intensity of the α phase compared with the β and γ phases increased with the nano-TiO_2 loading, which is consistent with the aforementioned FTIR spectroscopic result indicating that the α-phase crystal is dominant for PVDF/nano-TiO_2 composites.

Thermal Properties. The thermal stability of the neat PVDF film and PVDF/nano-TiO_2 composite films was characterized by TGA, as shown in Figure 7. For the neat PVDF film, the weight loss showed a single-step degradation pattern at ~440 °C with 60% loss. The incorporation of the nano-TiO_2 filler significantly lowered the degradation temperature to ~300 °C regardless of the amount of filler. This might be due to the fact that the nano-TiO_2 dispersed in the PVDF matrix sterically and entropically interfered with the secondary bonding interaction of macromolecular chains, resulting in decreased degradation temperature. The residue at 700 °C was proportional to the amount of nano-TiO_2 added, indicating the high thermal stability of nano-TiO_2 due to its high melting point (1,843 °C). The TGA results reveal that all the PVDF/nano-TiO_2 composite films were very thermally stable

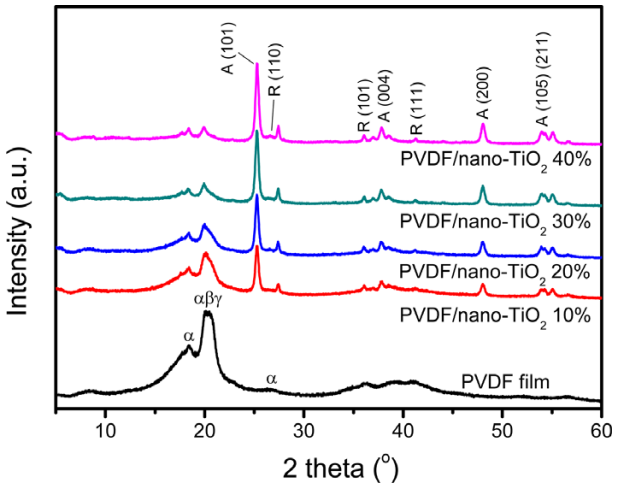

Figure 6. XRD patterns of neat PVDF film and PVDF/nano-TiO_2 composite films.

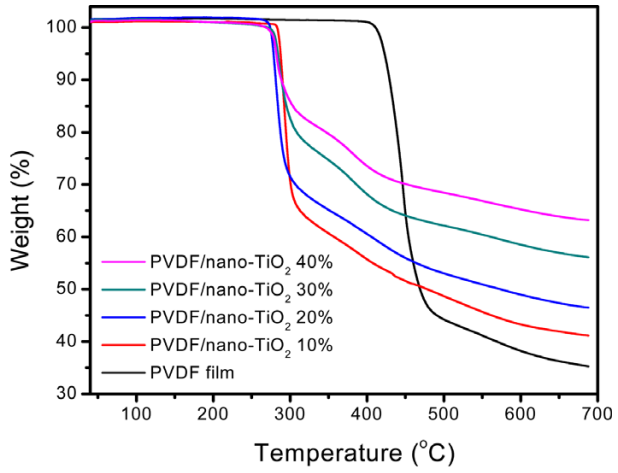

Figure 7. TGA curves of neat PVDF film and PVDF/nano-TiO_2 composite films.

up to 300 °C.

The thermal behavior of the neat PVDF film and PVDF/nano-TiO_2 composite films were also characterized by DSC measurements, as shown in Figure 8. The crystal-melting temperatures (T_m) of all samples are noted on the graph. The neat PVDF film showed a single T_m at 170.4 °C, which gradually decreased as the nano-TiO_2 content increased. This is because the incorporation of nano-TiO_2 fillers had an effect on the crystal phase of the PVDF to reduce efficient packing of macromolecular chains, which is consistent with the aforementioned FT-IR, density, and XRD results. The T_m gradually decreased from 170.4 to 160.8 °C for the composite with 30 wt% nano-TiO_2 loading, in which the α-phase crystal domain was predominant, as confirmed by the FTIR and XRD results. However, at 40 wt% nano-TiO_2 loading, the T_m slightly increased again, indicating the presence of a critical concentration of the filler. Excess amounts of nano-TiO_2 led to the partial aggregation of fillers and their segregation from the matrix due to their preferences for their own company, as revealed by SEM-EDS and density measurements.

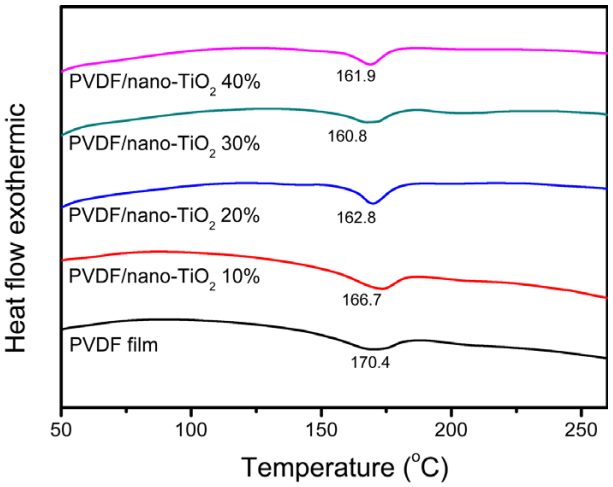

Figure 8. DSC curves of neat PVDF film and PVDF/nano-TiO_2 composite films.

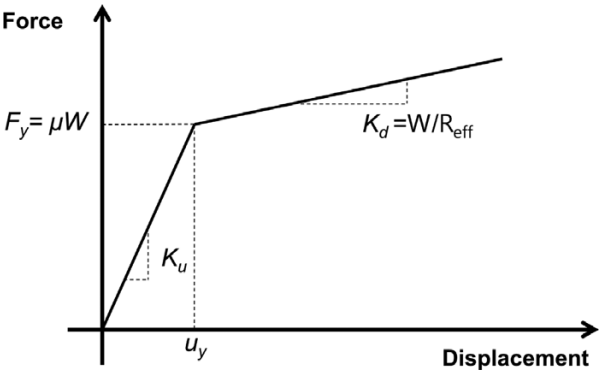

Figure 9. Simplified mechanical behavior of slider bearing.

Tribological Properties. Among the several mechanical properties, the friction coefficient is the main factor affecting the durability and capacity of the materials. A sliding bearing with a larger radius and friction coefficient can provide better performance owing to the greater characteristic force. Figure 9 shows the simplified mechanical behavior of the slider bearing. Here, R_{eff} is the radius of the slider, W is the weight of the superstructure, u_y is the yielding displacement, F_y is the yielding force, K_u is the initial stiffness, K_d is the yielding stiffness, and μ is the friction coefficient. The radius of the concave slider (R_{eff}) can elongate the fundamental period, and the friction coefficient is related to the durability or characteristic force of the isolation device. For an optimal and high-performance slider bearing, the frictional materials were developed based on PVDF/nano-TiO_2 composites. The results of the mechanical analysis, including the taber abrasion resistance and friction coefficient, are described as below.

The taber abrasion resistances of PVDF/nano-TiO_2 com-

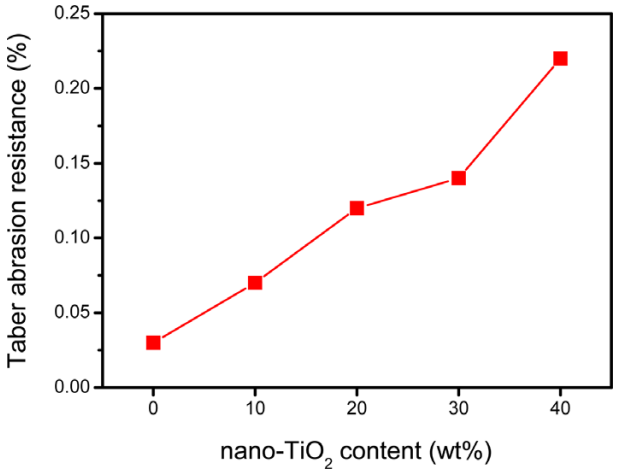

Figure 10. Taber abrasion resistances of neat PVDF film and PVDF/nano-TiO_2 composite films.

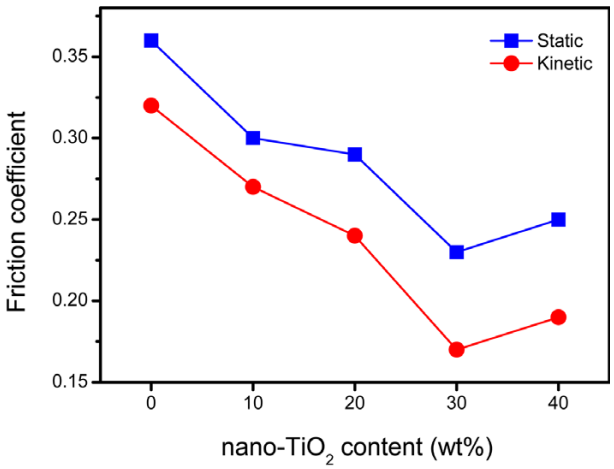

Figure 11. Static and kinetic friction coefficients of neat PVDF film and PVDF/nano-TiO_2 composite films.

posite films with various nano-TiO_2 contents are shown in Figure 10 and Table I. The wear property could be affected by the state of the surface. When the specimen started to wear, debris flew, and the agglomerates of the wear debris accumulated. Thus, the wear debris at the sliding interface introduced an additional term to the friction force. The wear resistance can be a key factor for economic feasibility. As the wear rate decreases, the durability and the maintenance period increase. Thus, for the design of the frictional material, the wear resistance should be considered as an economic aspect, in addition to the tribological performance. In particular, a low taber abrasion resistance is preferred to satisfy the standard of frictional materials. For the neat PVDF film without TiO_2, a good taber abrasion resistance of 0.03% was obtained owing to the large molecular weight and highly entangled chain structures. The taber abrasion resistance gradually and almost linearly increased with the amount of nano-TiO_2 filler. Most of the materials wore down at 40 wt% loading because of the aggregation of nano-TiO_2 fillers and their segregation from the PVDF matrix. The taber abrasion resistance of the commercialized ultra-high molecular weight polyethylene (UHMWPE) frictional material was ~0.1, demonstrating that all the PVDF/nano-TiO_2 composites had appropriate values, except at 40% nano-TiO_2 loading.

The friction coefficient is another very important parameter for developing frictional materials with high performance. The static and kinetic friction coefficients of PVDF/nano-TiO_2 composite films with various nano-TiO_2 loading values are shown in Figure 11 and Table I. The maximum variance from the average values was 0.011 and the error bound was approximately ±3%. Overall, the kinetic friction coefficients were lower than the static friction coefficients, but both coefficients showed the same tendency with respect to the amount of nano-TiO_2. Compared with the neat PVDF film, all the PVDF/nano-TiO_2 composite films exhibited improved (lower) friction coefficients. Two reasons for this improvement are suggested. First, the nonpolar α-phase PVDF crystal is dominant for the PVDF/nano-TiO_2 composites, as confirmed by FTIR and XRD analysis. It resulted in a decrease in the induced dipole-dipole moments, which could affect the interfacial

Table I. Taber Abrasion Resistance and Friction Coefficient of Neat PVDF Film and PVDF/Nano-TiO_2 Composite Films *via* Dry-Mixing and Uniaxial Hot-Press Molding Technique

Sample	Tabor Abrasion Resistance	Friction Coefficient (Dimensionless)		Note
		Static	Dynamic	
Neat PVDF	0.03	0.36	0.32	
PVDF/nano-TiO_2 10 wt%	0.07	0.30	0.27	
PVDF/nano-TiO_2 20 wt%	0.12	0.29	0.24	
PVDF/nano-TiO_2 30 wt%	0.14	0.23	0.17	
	-	0.24	0.16	Wet-mixing
PVDF/nano-TiO_2 40 wt%	0.22	0.25	0.19	
	-	0.30	0.19	Wet-mixing
Note	3,000 cycle	Frictional material - SUS304, Rate: 150 mm/min, Normal force ~2.25 N		

forces of adhesion. Second, nano-TiO_2 fillers could lessen the viscoelastic effects exhibited by the neat PVDF matrix. When rough materials slide over a viscoelastic polymer, a large amount of energy is dissipated owing to viscoelastic deformation, providing an additional component to the friction force. The addition of nano-TiO_2 fillers could improve the frictional performance by reducing the viscoelastic characteristics of the PVDF matrix. Furthermore, there is a great advantage in that both the friction coefficients are tunable and controllable according to the amount of nano-TiO_2 filler. Until 30 wt% nano-TiO_2 loading, the kinetic friction coefficient gradually decreased from 0.32 to 0.17 as the nano-TiO_2 content increased. However, both friction coefficients rebounded at 40 wt% loading, which can be explained by the third-body effects caused by the partial aggregation of the nano-TiO_2 fillers and their segregation from the PVDF matrix, as confirmed by density, SEM-EDS, and DSC analysis. Large amounts of fragile aggregation components might exist at high nano-TiO_2 loading, and thus the wear debris at the sliding interface could be an additional term for the friction force.

PVDF/nano-TiO_2 composite films with 30 wt% and 40 wt% nano-TiO_2 loadings were also prepared *via* a wet-mixing technique, which is known to be more effective for producing composites with intimate contact.[28,29] However, the wet-mixing process is more expensive, complicated and environmentally unfriendly compared to the dry-mixing process owing to the necessity of a large amount of solvent. For the wet-mixing process, PVDF and nano-TiO_2 powders were dissolved/dispersed in dimethylformamide at room temperature, and then the solvent was completely dried at 80 °C overnight. The same uniaxial hot-pressing method used for the dry-mixing process (190 °C at 20 MPa for 30 min) was applied. Interestingly, both static and dynamic friction coefficients of the PVDF/nano-TiO_2 composites with the dry-mixing technique were not significantly different from those of composites with the wet-mixing technique. It might be possible because 1) fine powders (both PVDF and nano-TiO_2) and 2) ultra-sonication process were used, which resulted in the homogeneous distribution and the intimate contact of each component.

Conclusions

A series of PVDF/nano-TiO_2 composite films with various nano-TiO_2 loading values up to 40 wt% were successfully fabricated by a dry-mixing and uniaxial hot-press molding technique. Nano-TiO_2 can function as an efficient filler to form α-phase crystal dominant composites. The nonpolar α-phase crystal domain of the PVDF contributed to improved frictional properties owing to the better contact adhesion. In addition, the incorporation of the nano-TiO_2 filler led to the reduced viscoelastic characteristic of the PVDF matrix, and as a result, the kinetic and static friction coefficients decreased to 0.17 and 0.23, respectively, at 30 wt% nano-TiO_2 loading. Moreover, the friction coefficient was controlled by adjusting the amount of nano-TiO_2 filler. However, at 40 wt% nano-TiO_2 loading, the fillers aggregated and segregated from the PVDF matrix, leading to the formation of fragile composites. The aggregation of the nano-TiO_2 fillers deteriorated the friction coefficients *via* wear debris at the sliding interface. Interestingly, the friction coefficients of the composites prepared by the dry-mixing technique were comparable to those of composites by the costly, environmentally unfriendly wet-mixing technique. This work demonstrates that the incorporation of nano-TiO_2 filler into the PVDF matrix *via* the dry-mixing technique is a cheap, effective strategy for improving the wear and friction properties of composites.

Acknowledgments. This work was supported by the Converged Energy Materials Research Center Program of the Defense Acquisition Program Administration and Agency for Defense Development, and a Korea Research Foundation Grant funded by the Korean Government (NRF-2014R1A2A2A09052374). Authors want to thank Mr. Ji-Hoon Moon at Yonsei University for the help in preparing specimens for the analysis.

References

(1) N. Degirmenbasi, S. Coskun, N. Boz, and D. M. Kalyon, *Fuel*, **153**, 620 (2015).
(2) S. Javdaneh, M. R. Mehrnia, and M. Homayoonfal, *Korean J. Chem. Eng*., **33**, 3184 (2016).
(3) G. Salimbeygi, K. Nasouri, A. M. Shoushtari, R. Malek, and F. Mazaheri, *Macromol. Res.*, **23**, 741 (2015).
(4) C. Basavaraja, J. K. Kim, and D. S. Huh, *Macromol. Res.*, **23**, 629 (2015).
(5) N. Shafaei, M. Jahanshahi, M. Peyravi, and Q. Najafpour, *Korean J. Chem. Eng*., **33**, 2968 (2016).
(6) W. Wu, J. Leng, Z. Wang, H. Qu, and J. Gao, *Macromol. Res.,* **24**, 209 (2016).
(7) P. Castaldo, B. Palazzo, and P. D. Vecchia, *Eng. Struct.*, **95**, 80 (2015).
(8) M. Eröz and R. DesRoches, *Eng. Struct*., **56**, 585 (2013).
(9) A. N. Sinitsin and V. V. Zuev, *Mater. Chem. Phys*., **176**, 152 (2016).
(10) B. Yang, L. Hu, R. Xia, F. Chen, S.-C. Zhao, Y.-L. Deng, M. Cao, J.-S. Qian, and P. Chen, *Macromol. Res.*, **24**, 74 (2016).
(11) A. Al-Kawaz, A. Rubin, N. Badi, C. Blanck, L. Jacomine, I. Janowska, C. Pham-Huu, and C. Gauthier, *Mater. Chem. Phys*., **175**, 206 (2016).
(12) Y.-H. Yun, J.-W. Yun, S.-D. Yoon, and H.-S. Byun, *Macromol. Res.,* **24**, 51 (2016).
(13) J. T. Shen, M. Top, Y. T. Pei, J. Th, and M. De Hosson, *Wear*, **322-323**, 171 (2015).
(14) J. H. Lee, S. J. Kim, J. S. Park, and J. H. Kim, *Macromol. Res.*, **24**, 909 (2016).
(15) A. Tang, M. Wang, W. Huang, and X. Wang, *Surf. Coat. Technol*., **282**, 121 (2015).
(16) N. Nemati, M. Emamy, S. Yau, J.-K. Kim, and D.-E. Kim, *RSC Adv.,* **4**, 19814 (2014).
(17) S. Sangeetha, G. P. Kalaignan, and J. T. Anthuvan, *Appl. Surf.*

Sci., **359**, 412 (2015).
(18) V. N. Aderikha, A. P. Krasnov, V. A. Shapovalov, and A. S. *Wear*, **320**, 135 (2014).
(19) M. Kalin, M. Zalaznik, and S. Novak, *Wear*, **332-333**, 855 (2015).
(20) L. Lin and A. K. Schlarb, *Tribol. Int.*, **101**, 218 (2016).
(21) A. Molazemhosseini, H. Tourani, A. Khavandi, and B. E. Yekta, *Wear*, **303**, 397 (2013).
(22) J. Tharajak, T. Palathai, and N. Sombatsompop, *Surf. Coat. Technol*., **273**, 20 (2015).
(23) W. S. Chi, R. Patel, H. K. Hwang, Y. G. Shul, and J. H. Kim, *J. Solid State Electrochem*., **16**, 1405 (2012).
(24) R. Moradi, S. M. Monfared, Y. Amini, and A. Dastbaz, *Korean J. Chem. Eng*., **33**, 2160 (2016).
(25) R. Moradi, J. Karimi-Sabet, M. Shariaty-niassar, and Y. Amini, *Korean J. Chem. Eng*., **33**, 2953 (2016).
(26) L. Zhu, Y. Wang, F. Hu, and H. Song, *Appl. Surf. Sci.*, **345**, 349 (2015).
(27) Q. Y. Peng, P. H. Cong, X. J. Liu, T. X. Liu, S. Huang, and T. S. Li, *Wear*, **266**, 713 (2009).
(28) Z. Y. Liu, K. Zhao, B. L. Xiao, W. G. Wang, and Z. Y. Ma, *Mater. Des*., **97**, 424 (2016).
(29) P. K. Ghosh, K. Kumar, and N. Chaudhary, *Compos. Part B: Eng*., **77**, 139 (2015).
(30) R. J. Nussbaumer, W. R. Caseri, P. Smith, and T. Tervoort, *Macromol. Mater. Eng.,* **288**, 44 (2003).
(31) P. Martins, A. C. Lopes, and S. Lanceros-Mendez, *Prog. Polym. Sci*., **39**, 683 (2014).
(32) S. Satapathy, P. K. Gupta, S. Pawar, and K. B. R. Varma, *Cornell University Library*, arXiv:0808.0419 (2008).
(33) L. Li, M. Zhang, M. Ronga, and W. Ruan, *RSC Adv.*, **4**, 3938 (2014).
(34) R. P. Vijayakumar, D. V. Khakhar, and A. Misra, *J. Appl. Polym. Sci*., **117**, 3491 (2010).
(35) A. Seema, K. R. Dayas, and J. M. Varghese, *J. Appl. Polym. Sci.,* **106**, 146 (2007).
(36) R. Li, C. Chen, J. Li, L. Xu, G. Xiao, and D. Yan, *J. Mater. Chem. A*, **2**, 3057 (2014).
(37) C. S. Lee, J. K. Kim, J. Y. Lim, and J. H. Kim, *ACS Appl. Mater. Interfaces*, **6**, 20842 (2014).
(38) C. S. Lee, J. Y. Lim, W. S. Chi, and J. H. Kim, *Electrochim. Acta*., **173**, 139 (2015).